Journal of Solid State Chemistry 181 (2008) 1546–1551

Contents lists available at ScienceDirect

Journal of Solid State Chemistry

journal homepage: www.elsevier.com/locate/jssc

Ag–Pt alloy nanoparticles with the compositions in the miscibility gap

Zhenmeng Peng, Hong Yang *

Department of Chemical Engineering, University of Rochester, Gavett Hall 206, Rochester, NY 14627-0166, USA

ARTICLE INFO

Article history:
Received 24 January 2008
Received in revised form
14 March 2008
Accepted 18 March 2008
Available online 26 March 2008

Keywords:
Ag–Pt alloy
Nanoparticle
Nanowire
Miscibility gap
Phase segregation

ABSTRACT

Silver platinum binary alloys with compositions between about Ag_2Pt_{98} and $Ag_{95}Pt_5$ at $<\sim 400\,^{\circ}C$ have largely not been observed in bulk due to the large immiscibility between these two metals. We present in this paper that Ag–Pt alloy nanostructures can be made in a broad composition range. The formation of Ag–Pt nanostructures is studied by powder X-ray diffraction (PXRD) and energy-dispersive X-ray (EDX). Our results indicate that lattice parameter changes almost linearly with composition in these Ag–Pt nanomaterials. In another word, lattice parameter and composition relationship follows the Vegard's law, which is a strong indication for the formation of metal alloys. Our transmission electron microscopy (TEM) study shows that the silver-rich Ag–Pt alloy nanostructures have spherical shape, while the platinum-rich ones possess wire-like morphology. The stability and crystal phase are investigated by annealing the alloy nanostructures directly or on carbon supports.

1. Introduction

Scaling-related thermodynamic property of bimetallic nanoparticles is of great current research interest because of the catalytic, magnetic and electronic applications of alloys and intermetallics [1–6]. With the decrease of particle size, especially to the point where the critical dimensions are in the nanometer regime, many properties can be significantly different from those of their bulk counterparts [4]. For example, surface plasmon resonance becomes significant for bimetallic Ag–Au nanoparticles and tunable with the change of compositions [7–11].

Although bulk phase diagrams for many bimetallic materials have been well studied and widely used for decades [12], it is unclear whether they can be simply extended to the nanometer-sized regime as a large fraction of atoms reside on the surfaces when sizes of particles become small. Surface atoms can contribute significantly to the increase of Gibbs free energy and result in a large difference in property between nanoparticles and bulk materials, such as melting point [13] and crystal order [14]. The large fraction of atoms on the surface and at interfaces of bimetallic nanoparticles should affect their phase behaviors, as being predicted by theoretical simulation [15–18]. In the case of Au–Ge alloys, both the composition and temperature of eutectic are shown to scale with the size of nanostructures [19]. Surface segregation of bimetallic nanoparticles is another phenomenon in which chemical composition at surface differs from that in bulk [20–23]. It becomes obvious when the difference in atomic size, surface energy, and strain energy between given two metal elements is large. The surface atoms can reconstruct to form core–shell [24–28], sandwich [21,29,30], and onion-like structures [31,32]. In this context, the miscibility of individual element in bimetallic nanoparticles is important in understanding the structure and property. Change in miscibility may help to design novel alloy nanomaterials possessing unique properties that may not be obtained as bulk materials.

Both theoretical studies and some limited experimental data have shown that miscibility between the metal elements can be increased with the decrease in particle size [15,16,18,33–35]. While nanoparticles of different alloys have been made, most of these materials have compositions existed in bulk forms [1,2,36,37]. Only a few nanoalloys with miscibility gaps have been observed, such as Au–Pt [38,39], Pt–Ru [40] and Pb–Sn [41]. The nanometer scale phenomena have hardly been explored. It is unclear if the enhancement of miscibility in these selective nanomaterials can be the case for Ag–Pt or other bimetallic systems. It is also interesting to study the meta-stability of these nanoalloys by examining the sintering behaviors of those bimetallic materials, if the miscibility is scalable with size.

We present in this paper the phase and composition behaviors of Ag–Pt nanoalloys. Silver platinum bimetallics have been studied in recent years as lead-free solder materials [42,43]. In the bulk, Ag–Pt bimetallics have a large miscibility gap at the temperature below about 1190 °C [12] and form alloys only at very high atomic content of either Ag or Pt [44]. When the atomic composition falls outside the range between Ag_2Pt_{98} and $Ag_{95}Pt_5$ at $<\sim$400 °C, the bulk materials exist in more than one phase: one Pt-enriched and the other Ag-enriched alloys. We show in this work that Ag–Pt alloy nanostructures can be synthesized in

* Corresponding author. Fax: +1 585 273 1348.
E-mail address: hongyang@che.rochester.edu (H. Yang).

0022-4596/$ - see front matter © 2008 Elsevier Inc. All rights reserved.
doi:10.1016/j.jssc.2008.03.013

solution from the molecular precursors of their corresponding salts. Furthermore, both miscibility and crystal phase of these nanoparticles can change upon annealing at 700 °C.

2. Experimental

2.1. Materials

Platinum acetylacetonate ($Pt(acac)_2$, Strem Chemicals, 98%) and silver stearate (Alfa Aesar) were purchased from VWR. Oleic acid (90%, technical grade), oleylamine (70%, technical grade), 1,2-hexadecanediol (HDD, 90%, technical grade), and diphenyl ether (DPE, 99%, ReagentPlus®) were purchased from Aldrich. All chemicals and reagents were used as received.

2.2. Synthesis

In a standard procedure, $Pt(acac)_2$ (0.03 g or 75 μmol), silver stearate (0.12 g or 0.30 mmol), HDD (0.49 g or 1.9 mmol) were mixed with oleic acid (0.3 mL or 0.9 mmol), oleylamine (0.3 mL or 0.9 mmol), and DPE (5 mL or 31.5 mmol) in a 25-mL three-neck round-bottom flask. The experiments were carried out under an argon atmosphere using the standard Schlenk line technique. A heating mantle was used in these reactions and the temperature was controlled by a thermal couple connected to a controller (J-KEM Scientific Inc.). The reaction mixture was heated to the reflux temperature (around 260 °C) at 5 °C/min and held for 1 h. To study the compositions, we systematically adjusted the relative amount between $Pt(acac)_2$ and silver stearate while kept the total mole number of these two precursors at 0.375 mmol.

After the reaction, nanoparticles were separated by dispersing the obtained reaction mixtures with 2 mL of hexane and 6 mL of ethanol, followed by the same centrifugation procedure mentioned above. The particles obtained were redispersed in 10 mL of hexane and 5 mL of ethanol, followed by centrifugation at 5000 rpm for 5 min. After this size selection the particles were collected for further study.

2.3. Thermal treatment

To study the phase behaviors during the annealing, both as-made and carbon-supported Ag–Pt nanoparticles were used. Several different loadings were examined for carbon-supported Ag–Pt nanoparticles. The heat treatment of these samples was conducted in a ceramic boat using a programmable tube furnace. The tube was heated to 300 °C in air at 5 °C/min and kept for 1 h, followed by ramping the temperature to 700 °C at 3 °C/min in forming gas (5 vol% H_2 in Ar). The annealing was conducted at 700 °C for 1 h.

2.4. Characterization

Powder X-ray diffraction (PXRD) patterns were recorded using a Philips MPD diffractometer with a Cu $K\alpha$ X-ray source ($\lambda = 1.5405$ Å). Transmission electron microscopy (TEM) images were taken on a JEOL JEM 2000EX microscope at an accelerating voltage of 200 kV. For TEM study, the specimens were prepared by drop-casting hexane-dispersed particles onto carbon-coated copper grids. Energy-dispersive X-ray (EDX) analysis was carried out on a field emission scanning electron microscope (FE-SEM, Zeiss-LEO DSM 982) operating at 20 kV. The SEM specimens, typically tens of micrometers in thickness, were prepared by transferring concentrated particle dispersions in hexane onto sample holders using pipettes. The thermal gravimetric analysis (TGA) was conducted on an SDT-Q600 TA instrument. In a standard procedure, 5–10 mg powder sample was transferred into an alumina pan, which was subsequently placed onto the dual beam sample holder. The flow rate of air was set at 50 mL/min. The typical temperature range was from room temperature to 800 °C and the heating rate was 10 °C/min.

3. Results and discussion

Silver platinum nanoparticles could be produced after a reaction period of 1 h for the reaction mixture at Ag stearate/$Pt(acac)_2$ molar ratio of 4:1 (Fig. 1a). The average diameter of these nanoparticles was about 8.2 nm with a standard deviation of 1.1 nm. When Ag stearate/$Pt(acac)_2$ molar ratio changed to 2:1, the particles obtained had a slightly larger average diameter of 9.2 ± 1.9 nm (Fig. 1b). The morphology of final particles became non-spherical, when Ag stearate/$Pt(acac)_2$ molar ratio decreased below above unity. Network of cross-linked nanowires was observed for the nanostructures formed at Ag stearate/$Pt(acac)_2$ molar ratio of 1:2 and 1:4 (Fig. 1c and d). The diameter of these nanowires was found to be about 6 nm. The large difference in particle morphology could be due to the surface segregation for the different compositions or a change in the growth kinetics with Ag stearate/$Pt(acac)_2$ ratio. In the later case, growth kinetic can be affected by the interactions between capping agents and surface atoms. Such interaction can be sensitive to the concentration of precursors and reaction condition.

Fig. 2 shows the PXRD patterns of these Ag–Pt nanostructures, pure silver (87-0719, JCPDS-ICDD) and platinum metals (70-2057, JCPDS-ICDD), respectively. All four Ag–Pt nanomaterials show diffractions that could be indexed to (111), (200), (220), (311) and (222) planes of a face-centered cubic (fcc) lattice. No other diffraction peak was observed, indicating these products were phase pure. The observed diffraction angles for Ag–Pt nanostructures fell in between those of the two pure metal elements, suggesting the formation of alloy nanoparticles. The diffraction

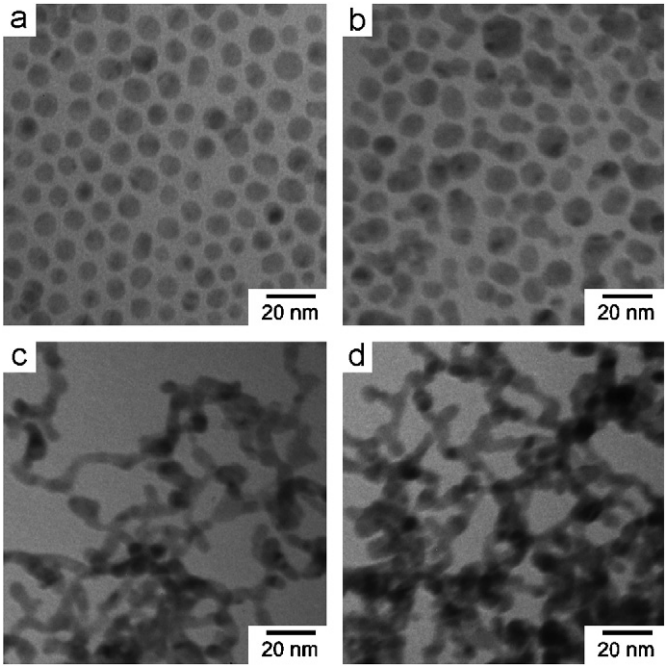

Fig. 1. TEM images of Ag–Pt nanoparticles made at different silver stearate/$Pt(acac)_2$ molar ratios: (a) 4:1, (b) 2:1, (c) 1:2, and (d) 1:4.

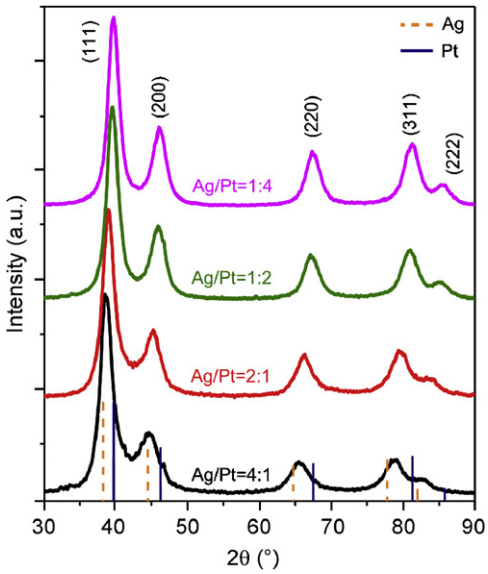

Fig. 2. PXRD patterns of Ag–Pt alloy nanoparticles made at different silver stearate/Pt(acac)$_2$ molar ratios.

peaks of alloy samples had higher 2θ angles than those for pure silver metal and moved to high angles with the decrease of Ag stearate/Pt(acac)$_2$ molar ratio.

EDX analysis was used to determine the elemental compositions for the final products. Platinum, silver, carbon and oxygen were the elements that could be detected, Fig. 3a. The carbon and oxygen signals were most likely due to the capping agents on the surfaces of nanoparticles. The atomic percentage of platinum in these bimetallic alloy products increased with the decrease in Ag stearate/Pt(acac)$_2$ molar ratio (Fig. 3b). The amount of silver in the nanoalloys seemed to be slightly lower than that in silver stearate used, suggesting that the silver precursors were not completely converted into alloy products after the reaction for 1 h.

A linear relationship between lattice parameter and composition described by the Vegard's law can be a good indication of miscible binary alloys that form solid solution. This relation can be described by the following empirical equation [45]:

$$a = a_2 \times \left(1 + \frac{a_1 - a_2}{a_2} \times x_1\right) \quad (1)$$

where a, a_1, and a_2 are lattice parameters for the binary solid solution and the two corresponding pure metals, respectively, and x_1 the molar fraction of Component 1. The lattice parameter for Ag–Pt alloys can be determined experimentally according to the following equation [46]:

$$a = \frac{\lambda}{2 \sin \theta} \times \sqrt{h^2 + k^2 + l^2} \quad (2)$$

where λ is the wavelength of X-ray which equals to 1.5405 Å for Cu $K\alpha$ source; θ the diffraction angle, and (hkl) the Miller indices. Fig. 4 shows the relationship between composition and lattice parameter of these Ag–Pt nanoalloys. The compositions were based on the EDX analysis and the lattice parameters were from the PXRD data. The average atomic compositions were $Ag_{74}Pt_{26}$, $Ag_{58}Pt_{42}$, $Ag_{26}Pt_{74}$ and $Ag_{16}Pt_{84}$, respectively, for alloy nanostructures made at the Ag stearate/Pt(acac)$_2$ molar ratio of 4:1, 2:1, 1:2 and 1:4. These experimental data agreed well with those theoretical values obtained based on the Vegard's law, indicating that the Ag–Pt particles were indeed alloys. The deviation between the experimental data and theoretical prediction might be largely due to the measurement errors although scaling effect

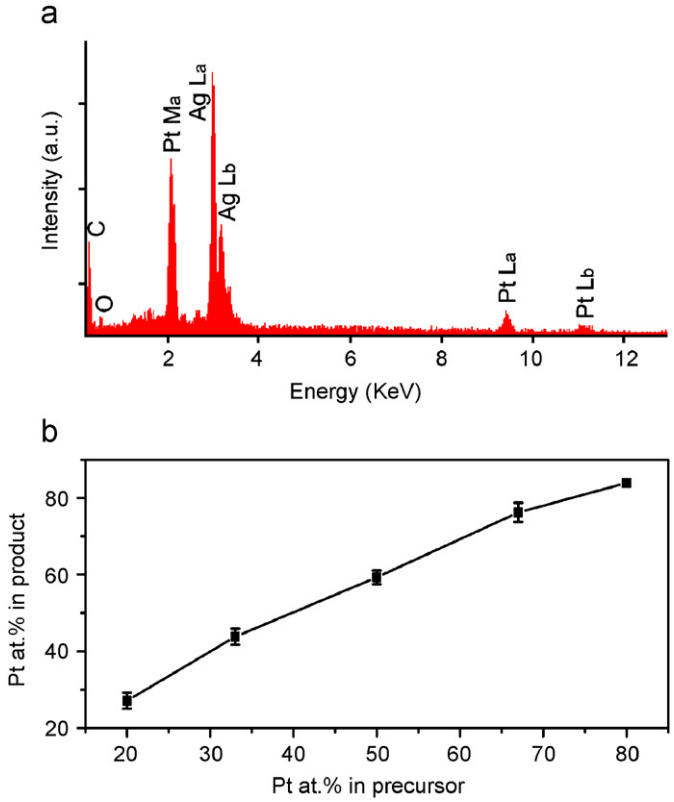

Fig. 3. (a) Representative EDX spectrum of Ag–Pt nanoparticles made with silver stearate/Pt(acac)$_2$ molar ratio of 4:1 and (b) relationship of platinum atomic percentage in Ag–Pt alloy nanostructured products and their corresponding metal precursors. Only the molar numbers of platinum and silver was considered in the calculation.

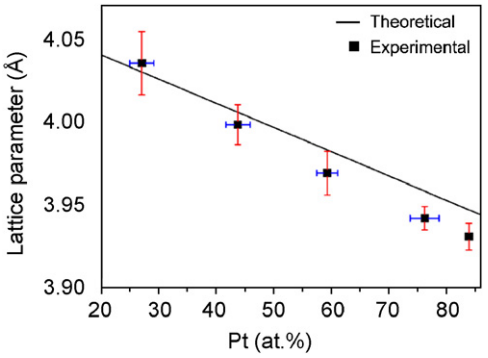

Fig. 4. Relationship between lattice parameter and composition of Ag–Pt binary alloy nanostructures. The theoretical values were calculated based on the Vegard's law.

could play a role in the calculation where bulk lattice parameters for pure metals were used. Recent studies suggest that 6 nm platinum and silver nanoparticles could have roughly 0.5% deviation in lattice parameter when compared with their bulks [47,48].

The effect of temperature on the phase stability of Ag–Pt nanoalloys were studied by treating the as-made particles at 300 °C for 1 h in air and then 700 °C for 1 h in the forming gas. The rationale for choosing 700 °C for the annealing experiments is that the phase transition and segregation for Ag–Pt nanoalloys occurs at around this temperature. In comparison, the phase transition temperature for the bulk Ag–Pt bimetallics is around 1200 °C [12]. Our TEM study indicates that the Ag–Pt nanoparticles sintered

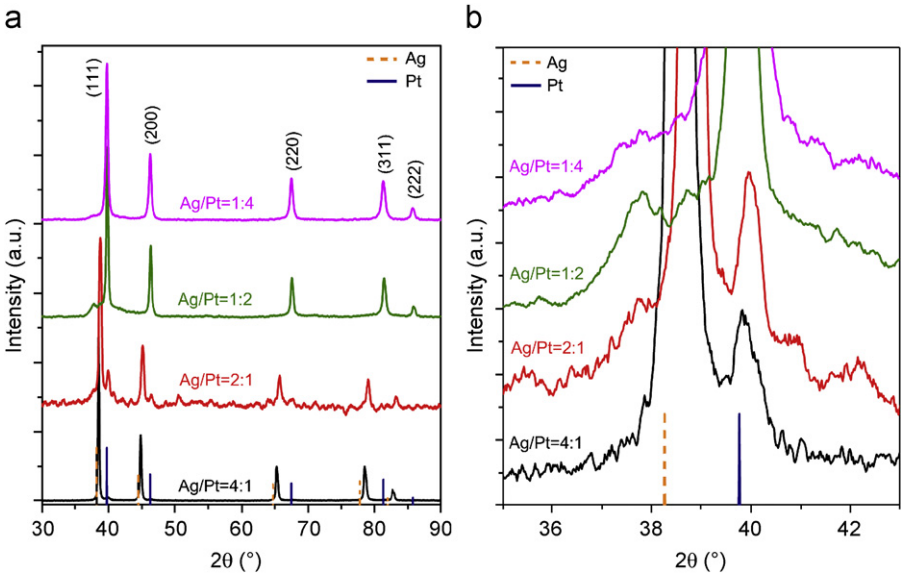

Fig. 5. PXRD patterns of thermally annealed Ag–Pt alloy nanostructures: (a) 30–90° 2θ range and (b) the enlarged (111) and (200) diffractions.

dramatically after the heat treatment. Fig. 5 shows the PXRD patterns of the sintered product from the four Ag–Pt alloy nanoparticles. The enlarged (111) diffraction regions were presented to show the change after this thermal treatment. For a given Ag–Pt alloy, at least one new set of diffraction peaks other than those for the alloy were detected, indicating that phase segregation happened. The relative peak intensities also changed with the atomic compositions of Ag–Pt alloy nanostructures. We noticed that the peak positions of these annealed products were not centered between those for pure silver and platinum metals, suggesting that Ag- and Pt-enriched alloys were most likely the main final products. The composition of these two enriched alloys should be near the phase boundary regions in the bulk phase diagram.

The $Ag_{74}Pt_{26}$ alloy nanoparticles were used to study the effect of particle size on the phase behavior. Carbon-supported alloy nanoparticles were also used to control the growth of particle size during the annealing process. The low, medium and high metal loadings were tested at 3, 10 and 70 wt%, respectively. Fig. 6 shows the TEM images of carbon-supported Ag–Pt nanoparticles at these three different loadings before and after the thermal treatment. At the low metal loading (3 wt%), the size of supported alloy particles do not change dramatically, as they were far apart. When the particle loading was increased to around 10 wt%, sintering became obvious. When the loading reached to around 70 wt%, the nanoparticles sintered in large numbers and formed crystals with the diameter or edge length up to several hundreds of nanometers.

Fig. 7 shows the PXRD patterns of these carbon-supported Ag–Pt nanoparticles after the thermal treatment. There were hardly any changes for the diffraction patterns at the low loading level of alloy nanoparticles. A careful examination shows that the diffraction peaks of these annealed Ag-enriched alloy nanoparticles were at higher angles than those after thermal treatment without carbon supports. This observation indicates that the carbon-supported Ag–Pt particles should have a less degree of phase segregation for samples with carbon supports than those without. In another word, the Ag–Pt alloy nanoparticles on carbon-support were thermodynamically stable at this enhanced

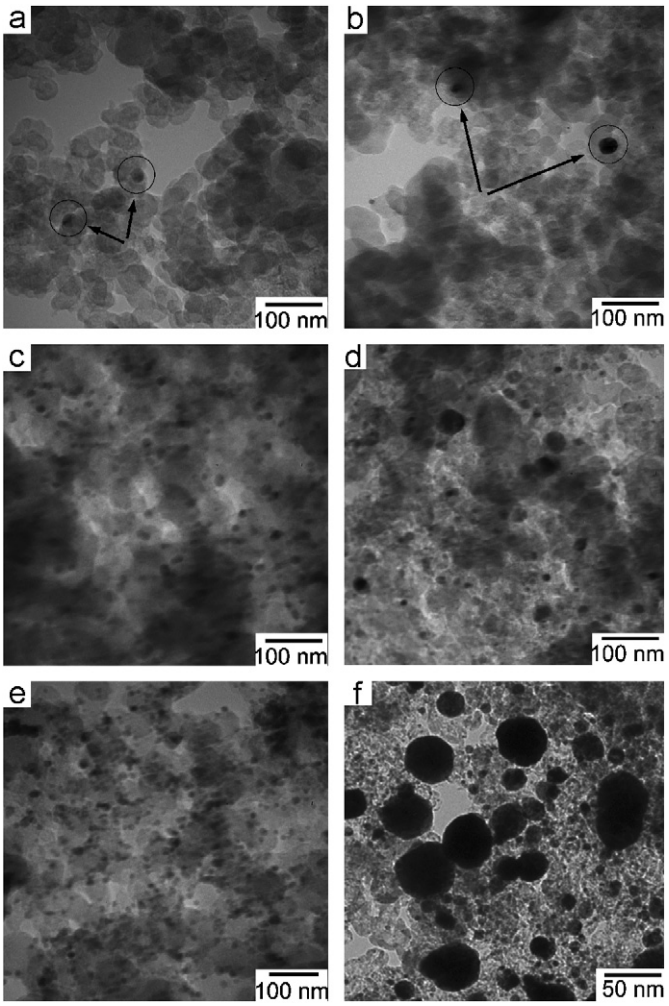

Fig. 6. TEM images of carbon-supported $Ag_{74}Pt_{26}$ nanoparticles at (a, b) 3, (c, d) 10, and (e, f) 70 wt% metal loadings (a, c, e) before and (b, d, f) after the thermal annealing.

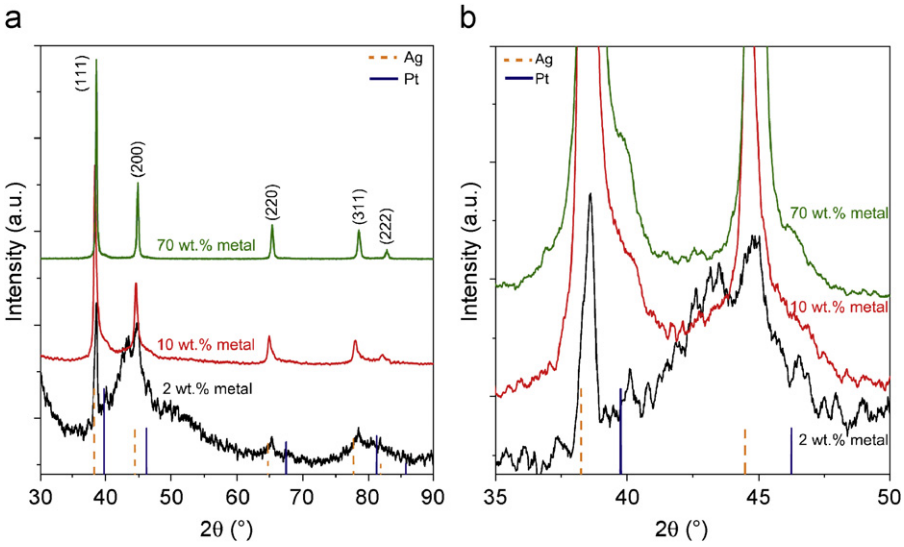

Fig. 7. PXRD patterns in (a) 30–90° 2θ range, and (b) for the enlarged (111) and (200) diffractions for carbon-supported $Ag_{74}Pt_{26}$ nanoparticles after annealing at 700 °C. The loading is based on the total weight of metals.

temperature and did not phase segregate as dramatically as the large particles during the annealing process. With the increase of metal loading, a shoulder peak around 40° 2θ and next to the (111) diffraction of Ag–Pt alloy appeared. Its position was close to the diffraction for pure platinum. The intensity of this shoulder peak increased with the metal loading on carbon support, indicating strong phase segregation after the annealing process. The diffraction peaks also became sharper than before due to largely the growth of crystal domain size, which agreed with the TEM observation.

4. Conclusion

Silver platinum alloy nanoparticles with composition through the entire miscibility gap of the bulk were successfully prepared. The lattice parameter and composition of these nanoparticles were experimentally determined and their relationship followed the Vegard's law, a strong indication of the alloy formation between platinum and silver at nanometer scale. These Ag–Pt alloy nanoparticles can grow in size and turn into two-phased solid-state materials after annealing at high temperature. These multiphase materials should be Pt- and Ag-rich alloys along the boundary regions in bulk phase diagram. Our PXRD and TEM data further suggest that the phase segregation of Ag–Pt alloy nanostructures could be size-dependent. Understanding of this phenomenon can be important for designing novel alloy nanomaterials, which may have unique electronic, magnetic and catalytic properties.

Acknowledgments

This work was supported by the US National Science Foundation CAREER Award (DMR-0449849).

References

[1] U. Jeong, X.W. Teng, Y. Wang, H. Yang, Y.N. Xia, Adv. Mater. 19 (2007) 33.
[2] S.H. Sun, Adv. Mater. 18 (2006) 393.
[3] A. Wieckoweski, E.R. Savinova, E.G. Vayenas, Catalysis and Electrocatalysis at Nanoparticle Surface, Marcel Dekker, Inc., New York, 2003.
[4] G.A. Ozin, A.C. Arsenault, Nanochemistry: A Chemical Approach to Nanomaterials, RSC Publishing, Cambridge, 2005.
[5] O. Koper, S. Winecki, in: K.J. Klabunde (Ed.), Nanoscale Materials in Chemistry, Wiley, New York, 2001, p. 263.
[6] Special Issue on Nanoalloys: From Theory to Application, Faraday Discuss. 138 (2008) 1.
[7] Y.G. Sun, Y.N. Xia, Science 298 (2002) 2176.
[8] Y.N. Xia, N.J. Halas, MRS Bull. 30 (2005) 338.
[9] B. Rodriguez-Gonzalez, A. Burrows, M. Watanabe, C.J. Kiely, L.M.L. Marzan, J. Mater. Chem. 15 (2005) 1755.
[10] R.A. Alvarez-Puebla, D.J. Ross, G.A. Nazri, R.F. Aroca, Langmuir 21 (2005) 10504.
[11] N.N. Kariuki, J. Luo, M.M. Maye, S.A. Hassan, T. Menard, H.R. Naslund, Y.H. Lin, C.M. Wang, M.H. Engelhard, C.J. Zhong, Langmuir 20 (2004) 11240.
[12] T.B. Massalski, J.L. Murray, L.H. Bennett, H. Baker, Binary Alloy Phase Diagrams, American Society for Metals, Metals Park, OH, 1986.
[13] S.F. Xiao, W.Y. Hu, J.Y. Yang, J. Phys. Chem. B 109 (2005) 20339.
[14] Y. Sun, L. Zhuang, J. Lu, X. Hong, P. Liu, J. Am. Chem. Soc. 129 (2007) 15465.
[15] A.S. Shirinyan, M. Wautelet, Mater. Sci. Eng. C—Biomimetic Supramol. Syst. 26 (2006) 735.
[16] A.S. Shirinyan, A.M. Gusak, M. Wautelet, Acta Mater. 53 (2005) 5025.
[17] A.S. Shirinyan, A.M. Gusak, Philos. Mag. 84 (2004) 579.
[18] M. Wautelet, J.P. Dauchot, M. Hecq, Nanotechnology 11 (2000) 6.
[19] H. Adhikari, A.F. Marshall, I.A. Goldthorpe, C.E.D. Chidsey, P.C. McIntyre, ACS Nano 1 (2007) 415.
[20] J. Tersoff, Appl. Phys. Lett. 83 (2003) 353.
[21] G.F. Wang, M.A. Van Hove, P.N. Ross, M.I. Baskes, Prog. Surf. Sci. 79 (2005) 28.
[22] D.S. Mainardi, P.B. Balbuena, Int. J. Quantum Chem. 85 (2001) 580.
[23] F. Lequien, J. Creuze, F. Berthier, B. Legrand, Faraday Discuss. 138 (2008) 105.
[24] S.J. Mejia-Rosales, C. Fernandez-Navarro, E. Perez-Tijerina, J.M. Montejano-Carrizales, M. Jose-Yacaman, J. Phys. Chem. B 110 (2006) 12884.
[25] H.B. Liu, U. Pal, R. Perez, J.A. Ascencio, J. Phys. Chem. B 110 (2006) 5191.
[26] D.J. Cheng, S.P. Huang, W.C. Wang, Phys. Rev. B 74 (2006) 064117.
[27] T. Van Hoof, M. Hou, Phys. Rev. B 72 (2005) 115434.
[28] D.S. Mainardi, P.B. Balbuena, Langmuir 17 (2001) 2047.
[29] F. Qin, C. Jiang, J.W. Anderegg, C.J. Jenks, B. Gleeson, D.J. Sordelet, P.A. Thiel, Surf. Sci. 601 (2007) 376.
[30] G.F. Wang, M.A. Van Hove, P.N. Ross, M.I. Baskes, J. Chem. Phys. 122 (2005) 024706.
[31] D.J. Cheng, W.C. Wang, S.P. Huang, J. Phys. Chem. B 110 (2006) 16193.
[32] F. Baletto, C. Mottet, R. Ferrando, Phys. Rev. Lett. 90 (2003) 135504.
[33] G. Ouyang, X. Tan, C.X. Wang, G.W. Yang, Nanotechnology 17 (2006) 4257.
[34] A. Shirinyan, M. Wautelet, Y. Belogorodsky, J. Phys.: Condens. Matter 18 (2006) 2537.
[35] H. Mori, H. Yasuda, Mater. Sci. Eng. A—Struct. Mater. Properties Microstruct. Process. 312 (2001) 99.
[36] R.E. Cable, R.E. Schaak, Chem. Mater. 17 (2005) 6835.
[37] R.E. Schaak, A.K. Sra, B.M. Leonard, R.E. Cable, J.C. Bauer, Y.F. Han, J. Means, W. Teizer, Y. Vasquez, E.S. Funck, J. Am. Chem. Soc. 127 (2005) 3506.
[38] G.C. Bond, Platinum Met. Rev. 51 (2007) 63.
[39] J. Luo, M.M. Maye, V. Petkov, N.N. Kariuki, L.Y. Wang, P. Njoki, D. Mott, Y. Lln, C.J. Zhong, Chem. Mater. 17 (2005) 3086.
[40] C.W. Hills, N.H. Mack, R.G. Nuzzo, J. Phys. Chem. B 107 (2003) 2626.
[41] J.G. Lee, H. Mori, Phys. Rev. Lett. 93 (2004) 235501.

[42] O. Nousiainen, T. Kangasvieri, K. Ronka, R. Rautioaho, J. Vahakangas, Soldering Surf. Mount Technol. 19 (2007) 15.
[43] O. Nousialanen, R. Rautioaho, K. Kautio, J. Jaaskelainen, S. Leppavuori, Soldering Surf. Mount Technol. 17 (2005) 32.
[44] F.N. Rhines, Phase Diagrams in Metallurgy: Their Development and Application, McGraw-Hill, New York, 1956.
[45] L. Vegard, H. Dale, Z. Kristallogr. 67 (1928) 148.
[46] E.W. Nuffield, X-ray Diffraction Methods, Wiley, New York, 1966.
[47] B. Medasani, Y.H. Park, I. Vasiliev, Phys. Rev. B 75 (2007).
[48] Q. Jiang, L.H. Liang, D.S. Zhao, J. Phys. Chem. B 105 (2001) 6275.